



Developing a 55% BTE Commercial Heavy-Duty Opposed-Piston Engine without a Waste Heat Recovery System

2017-01-0638

Published 03/28/2017

Neerav Abani

Achates Power Inc.

Nishit Nagar, Rodrigo Zermeno, Michael Chiang, and Isaac Thomas

Achates Power Inc

CITATION: Abani, N., Nagar, N., Zermeno, R., Chiang, M. et al., "Developing a 55% BTE Commercial Heavy-Duty Opposed-Piston Engine without a Waste Heat Recovery System," SAE Technical Paper 2017-01-0638, 2017, doi:10.4271/2017-01-0638.

Copyright © 2017 SAE International

Abstract

Heavy-duty vehicles, currently the second largest source of fuel consumption and carbon emissions are projected to be fastest growing mode in transportation sector in future. There is a clear need to increase fuel efficiency and lower emissions for these engines. The Opposed-Piston Engine (OP Engine) has the potential to address this growing need. In this paper, results are presented for a 9.8L three-cylinder two-stroke OP Engine that shows the potential of achieving 55% brake thermal efficiency (BTE), while simultaneously satisfying emission targets for tail pipe emissions. The two-stroke OP Engines are inherently more cost effective due to less engine parts. The OP Engine architecture presented in this paper can meet this performance without the use of waste heat recovery systems or turbo-compounding and hence is the most cost effective technology to deliver this level of fuel efficiency.

In this paper, engine performance results are presented for the 9.8L two-stroke OP Engine that employs currently available engine components, such as supercharger, turbocharger and after-treatment and features a uniquely designed piston bowl shape to enhance mixing with a swirl-to-tumble conversion as the piston bowls approach minimum volume. This design improves fuel-air mixing and hence, results in low soot values, increased indicated thermal efficiency (ITE) - due to better combustion phasing because of faster mixing controlled combustion, and lower NO_x because of improved area-to-volume ratio and lower fueling requirement per cycle. Results are presented from the two-stroke OP Engine-specific 1-D and 3-D CFD models developed for correlation to the three-cylinder 4.9L two-stroke research engine dynamometer measured data. These correlated models were used as tools to make predictions for the 9.8L heavy-duty engine. The optimized system includes a high trapped compression ratio piston bowl, ports design to provide best scavenging performance, thermal barrier coating on piston bowls and dual injector with an optimized spray pattern layout. Engine performance results are presented at three speed-load points. Results

show that the two-stroke OP Engine result in a BTE of 55%, while meeting stringent emission standards without the use of expensive waste heat recovery systems and/or turbo-compounding components.

Introduction

Heavy-duty trucks are the second largest and fastest growing segment of the U.S. transportation industry. Globally, emissions from heavy-duty vehicles are growing at a faster rate and are expected to surpass emission from passenger vehicles by 2030 [1]. As the fuel consumption from Class 8 Trucks using heavy-duty engines is expected to increase in the future, the need for commercially viable, clean and highly efficient heavy-duty engines is key to reducing GHGs.

The United States Department of Energy currently has in progress a Super-Truck Program [2] with industry partners with an objective to demonstrate 55% brake thermal efficiency by year 2020 [3,4,5,6]. Within the scope of the program, industry partners Cummins, Volvo, Navistar and Detroit Diesel have predicted BTE by simulating technologies for the future that include a waste heat recovery (WHR) system, advances in material that includes thermal-barrier coatings (TBC) to reduce heat transfer losses, friction improvement, combustion improvement that includes optimized piston bowl shape and injectors, and alternate fuel cycles. While several of these technologies impose additional cost, they have demonstrated via simulations respective contribution in reducing fuel consumption. In the field of alternative combustion strategies, Hanson et al. [7] and Kokjohn et al. [8] investigated fuel reactivity in a heavy-duty engine and could maximize indicated thermal efficiency in a single cylinder research engine. A similar concept was extended to investigate performance of reactivity controlled compression ignition on heavy-duty multi-cylinder engine [9] and a BTE of 47% was obtained. Menente et al. [10] investigated various fuels in a modified Scania 13L-1 heavy-duty single cylinder research engine and obtained an indicated efficiency between 52-55% at specific boost pressure and EGR levels.

Efforts from the Department of Energy, EPA and the industry are directed towards practical solutions to develop a highly efficient and clean heavy-duty engine for Class 8 trucks. The goal to achieve 55% brake thermal efficiency, while simultaneously meeting emissions standards for year 2020, will likely involve additional technologies, which will require additional components on the vehicle and add to the cost. Minimizing components and cost of the engine under this objective will be crucial for a developing a commercially viable engine for heavy-duty vehicles.

Opposed-Piston two-stroke Engines, currently in development at Achates Power, are lighter and more cost effective compared to conventional four-stroke engines and have potential for reductions in fuel consumption for many applications [12, 13, 14, 15, 16]. The specific design of the two-stroke OP Engine described here offers a solution to meeting the objectives of achieving a high BTE as well as meeting emissions standards without the use of waste heat recovery system and/or turbo-compounding. The fundamental benefits of OP Engines are discussed in detail by previous researchers [17]. A key summary of benefits of the two-stroke OP Engine architecture in achieving high BTE and clean emissions compared to a conventional four-stroke engine are as follows:

1. OP Engines have lower heat transfer losses as there is no cylinder head and the combustion chamber volume at the minimum volume is encompassed by the two-opposedpiston bowl.
2. Due to a lower BMEP requirement to achieve similar brake-power requirement as that of conventional four-stroke engine, two-stroke OP Engines operate leaner at a similar engine boost level. This results in higher thermodynamic efficiency due to the higher ratio of specific heat. Furthermore, OP Engines have larger combustion chamber volume with lower area-to-volume ratio for a given fuel amount required for a desired power output when compared to conventional four-stroke engines.
3. Achates Power two-stroke OP Engine include a piston bowl shape [18] that result in an enhanced mixing of fuel-spray and in-cylinder air motion, using both swirl and tumble components of flow. This leads to a faster heat released rate due to shorter mixing, controlled combustion duration and optimized combustion phasing which maximizes indicated thermal efficiency compared to a combustion chamber with only swirl component which is typically used in conventional four-stroke engines. Furthermore, due to side-injection, most of the spray plume mass penetrates near-parallel to combustion chamber surfaces compared to conventional four-stroke engines where due to central injection and swirl chamber most of the spray plume mass impinge upon the surface near-perpendicularly.
4. The opposed-piston engine flow, as an open-flow device during the scavenging process, introduces a fresh charge motion and does not have a dedicated pumping stroke like conventional four-stroke engines. This helps to optimize air handling components sizing resulting in lower pumping losses. Because of the overall less restrictive flow, EGR pumping is efficient.
5. The opposed-piston engine employs dual-fuel injectors with a narrower spray angle. This helps to reduce flame-wall interactions. Due to dual injectors, better rate shaping can be achieved compared to conventional engines.

6. Along with lower BMEP requirement, two-stroke OP Engines have full and independent control of internal and external cooled EGR. Intake and exhaust pressure are controlled independently of engine speed and load. This along with enhanced mixing controlled combustion leads to lower soot as well as lower engine-out NOx.
7. Two-stroke OP Engines have flat BTE map for wider range of loads and speeds. This enables the two-stroke OP Engine to provide better transient fuel efficiency.

While the above features are advantages of two-stroke OP Engines over four-stroke engines, the two-stroke OP Engine also has a clear advantage to conventional two-stroke engines as follows:

1. Lower surface area-to-volume ratio.
2. Uniflow scavenging without any use of poppet valves.
3. Higher scavenging time area for reduced pumping [14].
4. Higher stroke-to-bore ratio for improved scavenging.
5. Use of dual injectors instead of a central injector.

In this paper, results are presented that demonstrate the pathway to deliver 55% brake thermal efficiency using an opposed-piston two-stroke heavy-duty engine. First, correlation to measured dynamometer data for the two-stroke OP 4.9L multi-cylinder research engine are discussed followed by discussion on, design of the research engine, its air handling system and performance and emission development. Next, the correlated models are extended to predict performance for a 9.8L multi-cylinder heavy-duty two-stroke OP Engine. The unique way of operating the two-stroke OP multicylinder engine with thermal barrier coating shows a clear pathway for meeting 55% brake thermal efficiency at engine operating condition representing part-load conditions. Same engine also achieves 48% BTE at rated power conditions and 51% BTE at peak-torque conditions. Advanced technological concepts such as various waste heat recovery system have not been included in the predictions, which would increase the BTE further. Two-stroke OP Engines offer a commercially viable technology for heavy-duty engines that provides 55% BTE while simultaneously satisfying current emission standards.

Multi-Cylinder Two-Stroke OP Research Engine Specifications

The Achates Power two-stroke OP single cylinder research engine has been in testing since 2012 and the Achates Power two-stroke OP 4.9L three-cylinder research engine since 2014. The multi-cylinder research engine was originally designed to accommodate air-handling components that could provide flexibility in running various operating conditions, including very high power and high torque conditions. Because of this research engine, various torque and power requirements for different applications have been met investigated. More details on this OP research engine can be found in literature [1, 2, 3, 4, 5].

Table 1. Multi-cylinder OP research engine specification

Displacement	4.9 L
Arrangement, number of cylinders.	Inline 3
Bore	98.4 mm
Total Stroke	215.9 mm
Stroke-to-Bore Ratio	2.2
Compression Ratio	15.4:1
Nominal Power (kW @ rpm)	205 @ 2200
Max. Torque (Nm @ rpm)	1100 Nm @ 1200-1600

Air System for OP 4.9L Research Engine

Figure 1 provides an overview of the air-path for the three-cylinder two-stroke OP diesel engine. Upstream of the engine, a compressor driven by a fixed-geometry turbine is used to draw in fresh air. To aid the airflow across the engine, there is a supercharger driven by a two-speed drive. A supercharger bypass valve is used to control the airflow across the engine. The supercharger also acts as a pump to pull in the exhaust gases along the EGR loop. A venturi in the EGR loop, with a delta-pressure sensor is used to measure the EGR mass-flow. An EGR valve is used to control the EGR flow to the engine. Downstream of the engine, a back-pressure valve is used to simulate the back-pressure of a clean after-treatment system

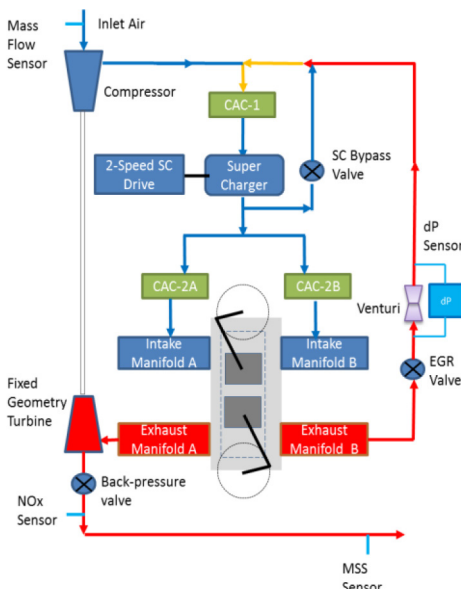


Figure 1. OP 4.9L research engine air handling system

Simulation Methodology

Two-stroke OP Engine simulations include the scavenging process coupled with combustion process, which entails coupling the multidimensional models with a one-dimensional model of two-stroke OP Engine. Accurate predictions of performance and emissions from an OP Engine depend upon the accuracy of the predicted trapped conditions. Trapped conditions can be decomposed into trapped flow conditions and trapped thermo-dynamic conditions. Trapped flow conditions include the three-dimensional velocity distribution inside the cylinder at the instant of port closure, as well as kinetic energy and turbulent dissipation distributions for the trapped turbulence. Trapped flow conditions are obtained by a 3-D CFD modeling of the scavenging process. Turbulence is modeled

through RNG k- ϵ model which has been widely used in engine combustion simulation. The scavenging results from 3-D CFD are passed onto 1-D model developed using commercial solver GT-POWER. These 1-D models predict trapped thermodynamic conditions, viz, trapped pressure, trapped temperature and trapped composition. Trapped thermodynamic and trapped flow parameters are then passed onto 3-D CFD engine combustion model.

To predict performance of the engine at a particular load and speed, a three-iteration loop calculation is carried out as shown in Figure 2. This enables accurate prediction of performance and emission parameters, such as NO_x and soot emission, indicated thermal efficiency (ITE), cylinder pressure and burn duration. In the first iteration, 1-D simulations provide boundary conditions to simulate the scavenging process using 3-D-CFD. In the second iteration, the results of scavenging CFD feeds back to the 1-D model that updates the 1-D predictions to generate thermodynamic trapped conditions. Next, trapped thermodynamic conditions are passed onto combustion CFD model. Trapped flow conditions are obtained from scavenging results obtained in the first iteration. At the second iteration, a swirl sensitivity study and a design of experiments (DOE) study is performed that finalizes the port orientation angle that determines the trapped swirl. New port geometries are developed to achieve desired target trapped swirl. A third iteration is needed to predict updated scavenging parameters based on the new port orientation that was designed in second iteration step using 3-D-CFD scavenging simulation. Once the trapped flow field and thermo-dynamic trapped parameters are updated, the engine combustion is simulated using 3-D-CFD scavenging simulation as well as 1-D tool predictions based on the new geometry and updated trapped conditions.

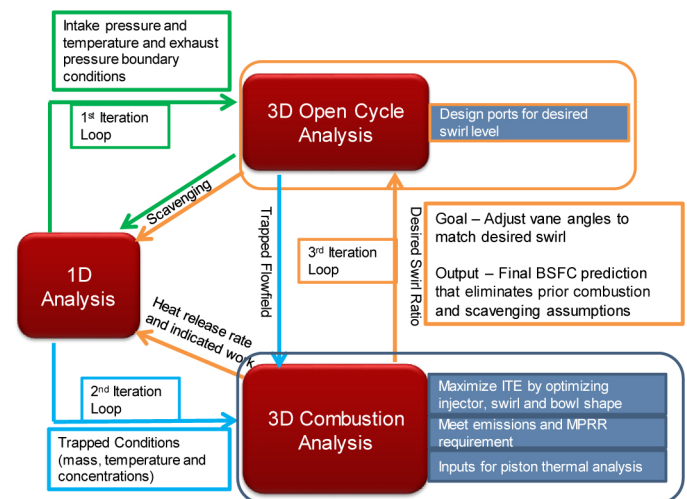


Figure 2. Schematic illustrating process of performance and emission optimization

The combustion CFD model includes a sub-model for sprays which has model constants specifically calibrated to simulate spray characteristics for the injector. These constants vary with injector types and are calibrated for each injector manufacturer. These model constants depend upon various nozzle hole parameters, such as L/D ratio, k-factor and discharge coefficient. For combustion correlation, performance parameters such as engine-out NO_x and soot emissions, ITE, cylinder pressure trace and burn duration are considered as essential metrics.

CFD Model Description

A modified version of the commercially available CONVERGE CFD software version 2.2 [19] is used to perform in-cylinder simulations of the two-stroke OP Engine combustion system. The modifications to the standard version of CONVERGE2.2 include user defined functions for simulating opposed-piston two-stroke motions, and computation of several performance, emissions and thermal management sub-models. Figure 3 shows the geometry of the Achates Power 4.9 L three-cylinder two-stroke OP Engine used in scavenging simulations. Figure 4 shows the surface geometry of the closed-cycle or combustion-cycle model with intake and exhaust pistons at their maximum separation for the third cylinder. The open-cycle simulations solve for blow-down event, scavenging process and models the closed-cycle. In this study, for open-cycle simulations, the computation time starts and ends from port-closure timing for the third cylinder for the entire 360-degree cycle. The calculations are repeated until the open-cycle simulation converges, which is when a converged trapped flow field is obtained. This trapped flow field is used as initial flow field for the closed-cycle simulation. The trapped pressure is specified based on the cylinder pressure measurements, and the trapped composition and temperature are obtained from correlated 1-D model for 4.9L multi-cylinder engine model to measurements using one-dimensional GT-POWER model predictions, as discussed before. Note that CONVERGE generates a volume mesh automatically at every time step. Both adaptive mesh refinement and fixed grid embedding techniques [14, 19] are employed to sufficiently resolve gradients in the flow-field and essential flow features.

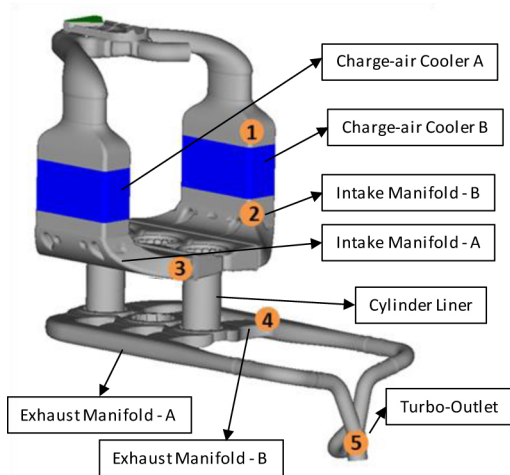


Figure 3. 4.9L multi-cylinder engine geometry considered for scavenging simulation. Label numbers are location of high speed pressure sensors.

To simulate engine combustion, an ERC n-heptane reduced chemistry mechanism was used to solve combustion chemistry which simulates n-heptane as a diesel fuel surrogate with 35 species and 77 reaction steps [20]. NO_x is calculated from a reduced NO_x mechanism [21] based on the GRI detailed NO_x reaction mechanism [22] sub-mechanism. Soot emissions are modeled using a two-step model, which includes a Hiroyasu formation step with acetylene as the precursor [23], and a soot-oxidation step based on Nagel-Strickland equation [24]. Sprays are modeled using a modified KHRT breakup model with RT break-up imposed in the near nozzle region as well along with a separate collision mesh for calculations for collision and coalescences [25,26]. The outcome of collisions are modeled using

O'Rourke collision model [26, 27] and in-cylinder turbulence is modeled using the RNG k- ϵ model [28]. Fuel injection rate profiles are specified based on measured data from a state-of-the-art, in-house fuel laboratory with IFR (Injection Flow and Rate) capabilities [29]. As with previous work on grid sensitivity studies for standard spray models [30], in this study mesh resolution in the range of 2 mm throughout the domain provided adequate qualitative and quantitative agreement with measured data, as well as the best optimum runtimes to achieve accurate correlation.

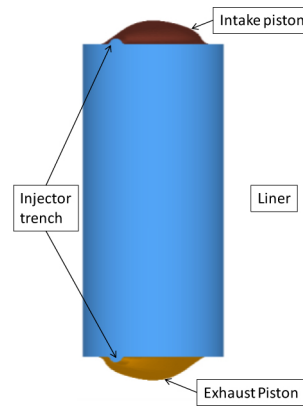


Figure 4. Closed-cycle geometry to simulate combustion CFD for 3rd cylinder.

Air System Development

The air system development for the two-stroke OP Engine includes designing air handling components and liner geometry. The air system of the multi-cylinder engine is developed by a coupling of 1-D models using GT-POWER and 3-D scavenging CFD model using CONVERGE2.2. Essential components of the two-stroke OP Engine that are designed through analysis as part of air system development are follows:

1. Super charger: This is used for controlling mass flow to be delivered to each cylinder and hence, trapped air-fuel ratio.
2. Super charger drive: This is designed for optimizing the pumping requirement for a given load-speed condition. For operating at peak efficiency at multiple load-speed conditions, the super charger may include a 2-speed drive.
3. Compressor: This is needed to find most appropriate compressor size in order for it to operate at maximum efficiency range.
4. Fixed geometry turbine: This is designed for most efficient pumping and the ability to deliver back pressure and mass flow rate.
5. Liner and port geometry: Both intake and exhaust port heights are designed based on the requirement of scavenging time area and blow-down time area for a given compression-ratio and expansion ratio. Port inclination is also designed to achieve required trapped swirl motion that is determined from open-cycle simulation.

Scavenging simulations for the multi-cylinder are carried out by imposing inflow boundary conditions at a location inside an intake manifold pipe just before the air cooler and outflow boundary conditions at the exhaust-turbo inlet. For cases used for model correlation to experiments, these locations have high speed pressure

sensors that provide transient pressure measurement. In case of model predictions, these boundary conditions are provided by the 1-D model which is solved in GT-POWER.

Performance and Emissions Development

Performance and emission development is based on CFD simulations of a closed-cycle and includes designing the following combustion hardware:

1. Combustion chamber shape
2. Total combustion volume to design required trapped compression ratio
3. Injector spray inclusion angle for dual injectors
4. Injector hole size
5. Number of injector holes
6. Port orientation angle to achieve required trapped swirl ratio needed for efficient and clean combustion.

As discussed previously, engine combustion is simulated using reduced chemistry mechanism and is simulated from port-closure to port-opening timings for closed-cycle simulations. This is performed for the third cylinder of the multi-cylinder engine. Trapped thermodynamic and trapped flow parameters are passed onto the 3-D CFD engine combustion model after convergence of 3-D CFD and 1-D simulation results. A design of the experiment is undertaken to optimize combustion system for maximum ITE that can also satisfy emission requirements.

Results and Discussion

Results are presented in the next two sub-sections. First, results are presented for CFD model correlation to measurement data for the two-stroke OP 4.9L engine. The measurements were conducted on multi-cylinder engine test dynamometer. In the second sub-section, combustion performance results and brake thermal efficiency predictions are presented for the 9.8L engine using the correlated model.

Results: CFD Model Correlation to OP 4.9L Research Engine Dynamometer Measurements

The CFD model has been well correlated to the three-cylinder 4.9L two-stroke OP research engine. In this sub-section, results of open-cycle CFD correlation and combustion CFD correlation to the data for the 4.9L engine are discussed. Although the CFD correlation is discussed in this paper, the process described in the previous section where CFD and 1-D models are coupled, have been used to design the hardware being used in the 4.9L research engine dynamometer testing [14, 15, 16]. The developmental process of CFD led hardware design, CFD correlation and CFD model improvements has evolved with several cycles for wide range of hardware testing as well as wide range of OP Engine sizes. These models have been shown to provide accurate performance predictions of two-stroke OP Engines for various applications. The two-stroke OP Engine specific models have demonstrated that combustion hardware designed based on these models has resulted engine performance metrics that agree with predictions in the design stage. In this section, results are presented for the correlation of these OP Engine specific developed CFD models with measurement.

Open-Cycle CFD Correlation

Open-cycle CFD correlation is an important task that feeds both the 1-D tool to predict cycle BSFC, as well as the 3-D combustion CFD models to provide trapped flow conditions. The open-cycle model includes simulation of entire 360 degree cycle that comprises of blow-down event, scavenging event and closed-cycle event. To capture closed-cycle event as part of open-cycle simulations, a simple model that imposes a given cylinder pressure as well as captures transient adiabatic index variation during combustion event simulated the closed-cycle event. This accurately predicts the in-cylinder conditions during blow-down when the exhaust port is open, as well as during scavenging when both intake and exhaust ports are open. [Appendix-I](#) describes various scavenging parameters that are used in the correlation. Delivery ratio and trapped cylinder pressure are the measured parameters that can be directly compared with predictions. [Figure 5](#), [Figure 6](#), [Figure 7](#), [Figure 8](#), [Figure 9](#), show the comparison between the CFD predictions and measured data for pressure vs crank angle at various locations in the intake and exhaust manifolds at A75 mode for the 4.9L research engine which represents 1400 RPM and 75%load. As can be observed the predicted pressure agrees well with measurements that confirm that the models are well correlated and can capture pressure-wave dynamics reasonably well. The predicted mass delivered to the engine was within 2% compared to measurement.

The converged CFD solution from the open-cycle also predicts the trapped swirl motion, which is the trapped flow field used in the 3-D CFD combustion simulations. Results from the CFD open-cycle correlation can be summarized as a scavenging schedule as well, and passed onto a 1-D model, which provides trapped thermodynamic conditions. After convergence and verification of correlation with the open-cycle and 1-D model, the combustion CFD correlation comes as a next step, which will be discussed in the next section.

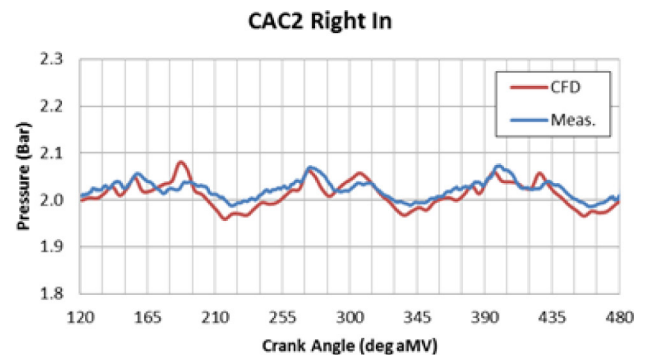


Figure 5. CFD predictions of pressure at inlet of right-side Charge Air Cooler [Location 1] at A75.

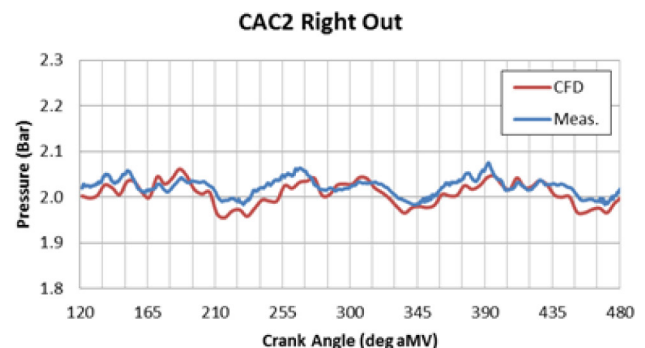


Figure 6. CFD predictions of pressure at outlet of right-side Charge Air Cooler [Location 2] at A75.

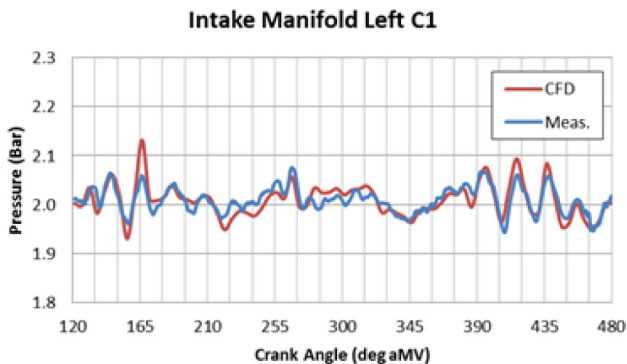


Figure 7. CFD predictions of pressure at left-side in Intake Manifold [Location 3] at A75.

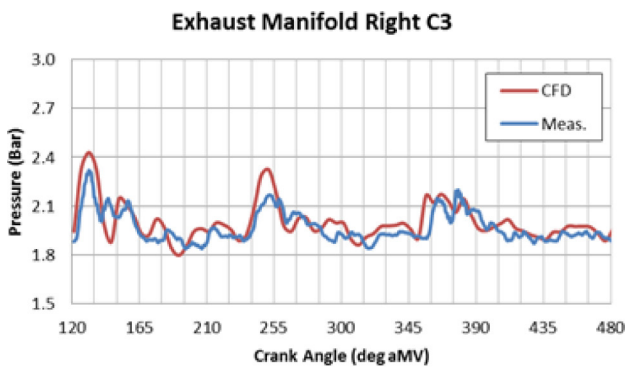


Figure 8. CFD predictions of pressure at right-side in Exhaust Manifold [Location 4] at A75.

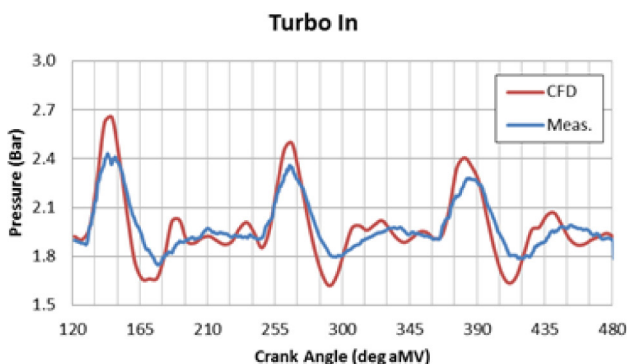


Figure 9. CFD predictions of pressure at inlet of Turbine [Location 5] at A75.

Combustion CFD Correlation

Combustion CFD models are correlated at two load and speed points; 75% load at 1400 rpm (A75 mode) and 75% load at 2200 rpm (C75 mode). The spray sub-model constants essentially are specific to each injector and each OEM. The spray sub-models have been correlated based on achieving accurate emission and cylinder pressure predictions on mesh size around 2-3 mm in the domain. The soot model constants were also anchored to provide the accurate predictions of soot measurement at both these load points.

Figure 10 shows the comparison of CFD predictions of the incylinder pressure and instantaneous heat released rate compared to measurements at A75 mode. The measured heat released rate is apparent heat released rate and the CFD predicted heat released rate is scaled to match the apparent heat released as derived from measurements. Table 2 shows the comparison between predictions and laboratory measurements of emissions, closed-cycle work

(PdV_CC), burn duration (CA10-90) and indicated thermal efficiency (ITE). Overall the predictions compare well with measurements. Similar comparison for C75 mode are shown in Figure 11 and Table 3 indicate that predictions of emissions and ITE compare well with measurements.

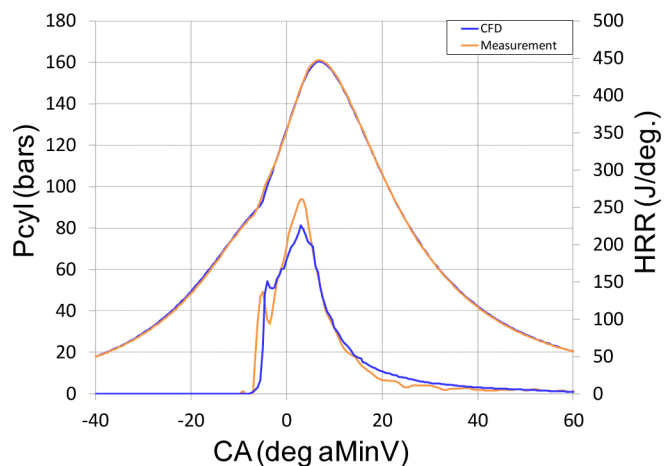


Figure 10. Comparison of in-cylinder pressure and heat released rate with measurement at A75 for three-cylinder OP 4.9L research engine

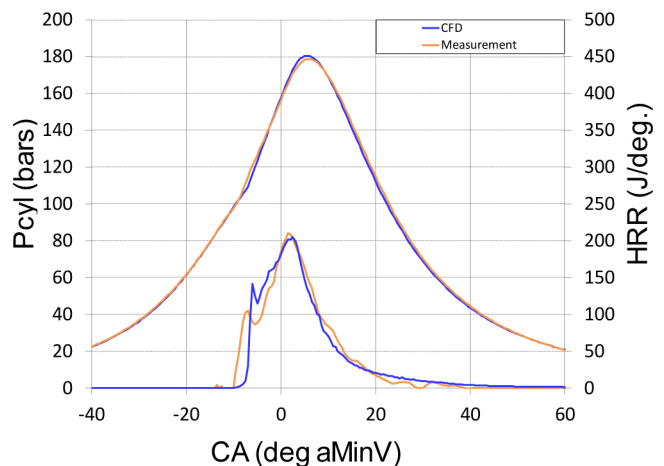


Figure 11. Comparison of in-cylinder pressure and heat released rate with measurement at C75 for three-cylinder OP 4.9L research engine

Table 2. Performance comparison of predicted vs measurements at A75 for three-cylinder OP 4.9L research engine

A75	Soot (gms/kgf)	NOx (gms/kgf)	Pdv_CC (kW)	CA10 (° ca)	CA50 (° ca)	CA90 (° ca)	CA1090 (° ca)	ITE [%]
CFD	0.077	19.9	45.2	-3.0	4.0	24.0	27.0	50.0
Measurement	0.089	19.7	45.1	-3.0	4.0	18.5	21.5	49.7

Table 3. Performance comparison of predicted vs measurements at C75 for three-cylinder OP 4.9L research engine

C75	Soot (gms/kgf)	NOx (gms/kgf)	Pdv_CC (kW)	CA10 (° ca)	CA50 (° ca)	CA90 (° ca)	CA1090 (° ca)	ITE [%]
CFD	0.084	10.59	62.0	-5.0	2.5	18.0	23.0	51.6
Measurement	0.082	10.53	63.2	-5.0	3.0	14.0	19.0	52.6

Friction Model Correlation

A friction model was constructed, which includes losses from the power cylinder, gearbox, crank bearings, engine auxiliaries and seals. The power cylinder and crank bearing friction was calculated using a crank angle resolved model which allows for impact of the cylinder pressure history to be included in assessing the friction for these components.

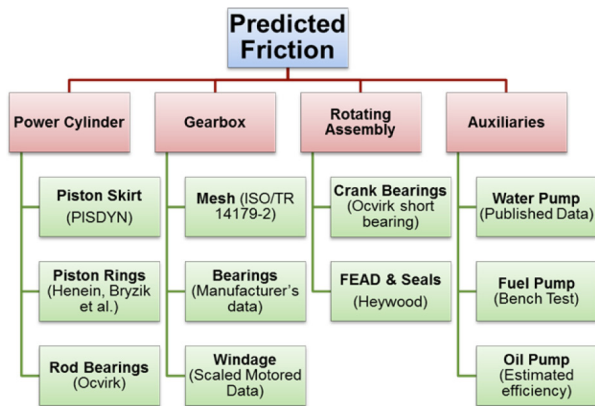


Figure 12. Overview of Friction Model

Figure 12 provides an overview of the sub-system models that were utilized in order to determine engine friction. Ricardo PISDYN was used to model piston secondary motion, dynamic land clearance and skirt friction. PISDYN includes a 3-D elasto-hydrodynamic model of the oil film between the skirt and liner and takes into account the operating conditions such as cylinder pressure, skirt geometry and skirt profile. The piston ring friction model was developed based on work published by Henien, et al [31, 32, 33]. This model accounts for transients by considering crank resolved effects for engine geometry, ring profile, liner temperature and cylinder pressure. The crank bearing model is based on short bearing theory [33, 34]. In this model the bearing loads due to gas pressure force and component inertial forces are calculated at each crank angle in order to calculate friction loss. The gear mesh losses were modeled using ISO/TR 14179-2 technical report [35]. The model calculates an average friction coefficient as a function of loading, tooth geometry, oil viscosity, surface finish and a lubricant factor. Power loss is then calculated as a function of input power, friction coefficient, and a tooth loss factor. The roller bearing losses were calculated using the data provided by the manufacturer. Geartrain windage loss was estimated using gear spin test data and a simple model was developed to scale the power loss with gear geometry

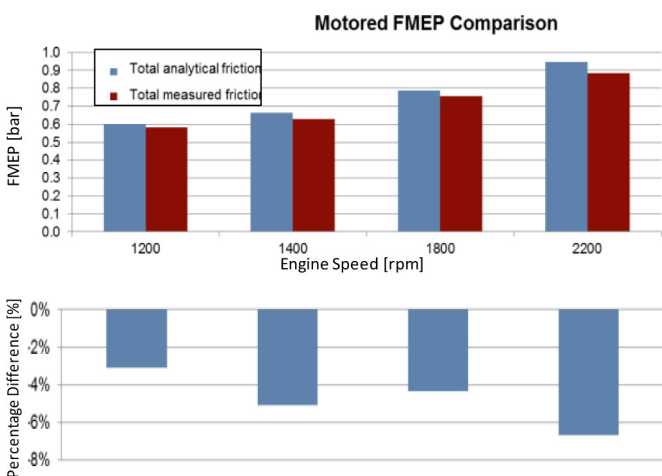


Figure 13. Comparison of measured vs predicted motored FMEP for three-cylinder OP 4.9L research engine

The total friction model was then compared to measured motored and the calculated fired friction of the engine to assess its validity. An important thing to note here is that neither load nor speed dependent constants have been used to correlate the model results with

measurement. Figure 13 shows the comparison of measured motored friction vs analytically predicted friction. As it can be seen, the model is able to predict friction within 7% of the measured motored friction.

The next step was to check the performance of the model in fired condition. The engine fired friction power was calculated by subtracting the supercharger power and brake power from indicated power. This was compared to the prediction from the friction model. The results are shown in Figure 14. The analytical model is able to predict friction within +/- 10% range for most of the load speed points. The error is on higher loads, however, since friction power overall is a smaller fraction of fuel power at higher loads, the overall impact on BSFC prediction is marginal. As is evident from the measured data, the measured engine friction is high. This is because the 4.9L engine was developed as a research platform and was overdesigned with available off-the-shelf components. Some of the features that contribute to high engine friction are - an external gearbox with overdesigned gears and power take-off from central gear, oversized lube and water pump, older generation off-the-shelf ring pack, non-optimized crankshaft, bearing and a Front End Accessory Drive (FEAD). Knowledge of these causes for the higher friction of the research engine represents a known course of action for reducing friction in a more realistic production type engine.

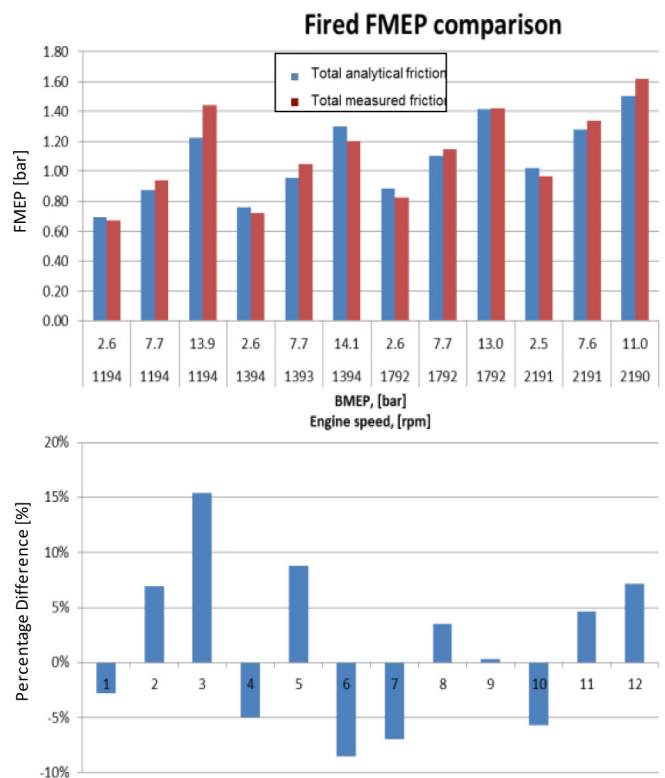


Figure 14. Comparison of analytically predicted and measured friction for three-cylinder OP 4.9L research engine

Results: API 9.8L, Three-Cylinder Two-Stroke OP Heavy-Duty Engine

As discussed in the previous section, the two-stroke OP Engine specific multi-dimensional models give excellent correlation to measured data. These models have been used for designing engine components pertaining to air system and combustion system and have resulted in accurate predictions [15]. In this section, predictions are presented from these models for a two-stroke OP 9.8L heavy-duty

engine. The predictions were made by extending the combustion CFD model used for 4.9L research engine correlation, as discussed in the previous sub-section. Due to the requirement for a larger number of computational cells, because of larger bore diameter, the computational time was higher since the mesh resolution was kept in the range of 2-3 mm of range during combustion event.

OP heavy-duty engine development includes developing operating conditions, designing ports that satisfy both pumping targets as well as the trapped charge motion requirements, developing piston bowl shape, and injectors to provide maximum ITE. The design process of 9.8L three-cylinder heavy-duty engine followed the process illustrated in [Figure 2](#). In the next sub-sections, details of scavenging optimization, port heights investigation, operating conditions for the heavy-duty engine, and combustion system optimization will be discussed. The engine details are shown in [Table 4](#). Unlike a conventional four-stroke engine, the two-stroke OP Engine does not require to be down-spiced to deliver higher efficiency. As a result, there is no necessity for very high torque at lower RPM speed resulting in simplification and cost saving for transmission and axle.

Table 4. Multi-cylinder two-stroke OP heavy-duty engine specification

Displacement	9.8 L
Arrangement, number of cylinders.	Inline 3
Bore	120 mm
Total Stroke	288 mm
Stroke-to-Bore Ratio	2.2
Optimized Compression Ratio	21:1
Rated Power (kW @ rpm)	340 kW @ 1800
Max. Torque (Nm @ rpm)	2100 Nm @ 1200-1400

The air system layout is shown in [Figure 15](#). It is very similar to the A48-3 research engine with the addition of a low pressure EGR loop. For lower loads (50% or less), the low pressure EGR loop helps in maintaining the desired EGR rate while improving the overall turbocharger efficiency, thus lowering the pumping losses.

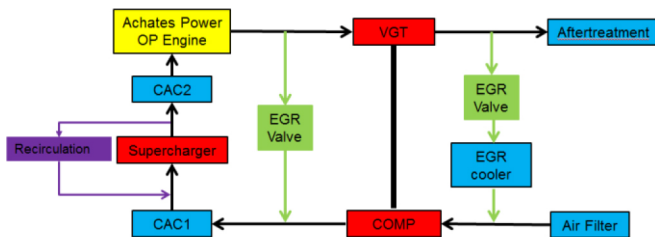


Figure 15. Air system layout for 9.8L heavy-duty two-stroke OP Engine

Typically, the most weighted point for a heavy-duty engine is around part-load conditions with engine speed of 1200 RPM at 50% load representing a break-power in the range of 120-130 kW. This are the conditions where the long-haul truck spends significant portion of time. As a result, part-load point of 1200 rpm and 50% load point was chosen for combustion system optimization, scavenging simulations, prediction of flow field, and 1-D predictions thermodynamic trapped conditions. A DOE study to optimize the combustion system was also performed at this load-speed point; details of which will be discussed in next sub-section. Furthermore, rated-power and peak-torque conditions were also investigated to ensure that the heavy-duty two-stroke OP 9.8L optimized engine delivers 342kW and 255 kW,

respectively at these conditions with PCP limit of 235 bar. [Table 5](#) shows various engine speed-load conditions investigated for 9.8L engine performance

Table 5. Two-stroke OP Engine speed-load selected for combustion optimization and predictions

Mode	Engine	Power
[-]	[rpm]	[kW]
Part Load	1200	128
Rated Power	1800	342
Peak Torque	1200	255

Scavenging Optimization

Scavenging simulations and optimization were performed with an objective of improving scavenging efficiency (SE) while maximizing trapping efficiency (TE). These were optimized along with a scavenge ratio that governs the pumping requirement of the engine. The result of the scavenging optimization determined port height, scavenge ratio for a given load-speed point, scavenging efficiency and trapping efficiency. In this study, scavenging performance is compared for several port heights and the best performing ports are investigated for its effect on combustion performance. Combustion optimization provides the requirement of trapped swirl motion that depends upon the port inclination. The outcome of combustion optimization along with scavenging optimization determines port design.

Table 6. Boundary conditions for scavenging simulations for ports obtained from 1-D model

Condition	Port-A	Port-B
RPM	1200	1200
Torque [Nm]	1022	1022
Boost [bar]	1.79	1.64
Global AFR [-]	26.0	26.1
EGR Rate [-]	29%	29%
Pumping loss [% fuel energy]	1.0	1.3

Port Heights Investigation

Two ports were evaluated namely port-A and port-B that have port lift profile as shown in [Figure 16](#). Port lift for two-stroke OP Engines are defined by transient port area change determined by the piston motion profile. Port-A design has bigger ports and port-B has smaller ports. The boundary conditions for CFD simulations came from the 1-D simulation results from GT-POWER tool, as shown in [Table 6](#). The size of the ports determines the pumping, trapped temperature and the orientation determines the engine swirl. Using both the ports, the combustion system was optimized and a comparison was made as to which combination of ports and combustion systems provides the best ITE. [Figure 17](#) show the boundary conditions for port-A and port-B as generated by 1-D model as part of the 1st iteration. Results show that bigger ports will result in lower pumping loss but slightly lower scavenging efficiency, as observed in [Figure 18](#) and [Figure 19](#) for the two ports, respectively. Based on data for scavenging performance from [Table 7](#), port-B results in improved scavenging, lower trapped temperature and higher trapped swirl.

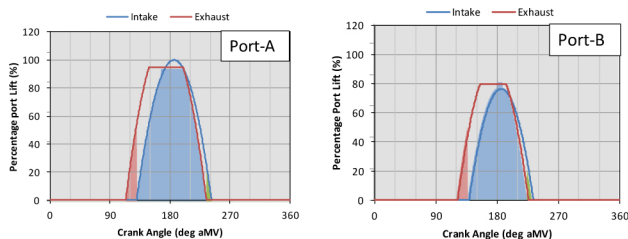


Figure 16. Port lift profile for Port-A and Port-B.

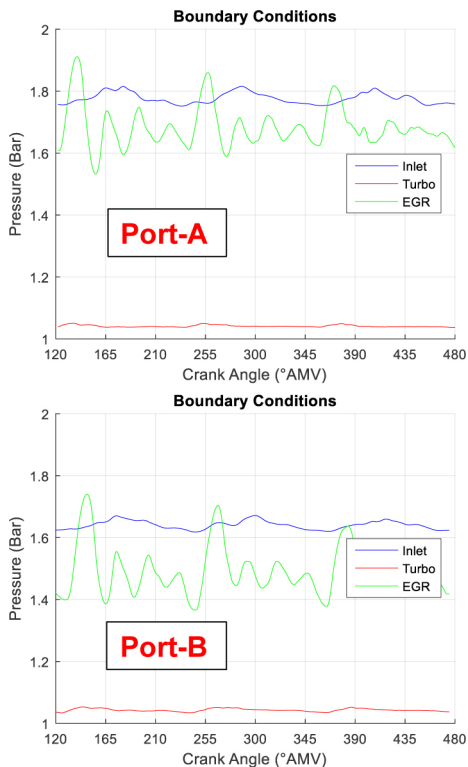


Figure 17. Transient pressure boundary conditions obtained from 1-D model and used for scavenging simulations for two ports

Table 7. Scavenging performance comparison of port-A and port-B from open-cycle CFD simulations. Definition for various terms in show in table are specified in Appendix-I

Port-A 1200RPM 50%								
Description	DR	CE	SE	SR	RC	TE	Temp@PC	Swirl@PC
Unit	(-)	(-)	(-)	(-)	(-)	(-)	(K)	(-)
C1	1.051	0.984	0.825	0.882	1.192	0.936	392.6	-1.7
C2	1.084	0.972	0.816	0.910	1.191	0.897	391.7	-1.7
C3	1.060	0.923	0.802	0.921	1.151	0.871	404.1	-1.6
Average	1.065	0.960	0.815	0.904	1.178	0.901	396.1	-1.7
Range	3.0%	6.3%	2.9%	4.3%	3.4%	7.1%	3.1%	-5.1%

Port-B 1200RPM 50%								
Description	DR	CE	SE	SR	RC	TE	Temp@PC	Swirl@PC
Unit	(-)	(-)	(-)	(-)	(-)	(-)	(K)	(-)
C1	1.041	0.982	0.833	0.883	1.179	0.944	380.0	-2.4
C2	1.086	1.008	0.839	0.903	1.202	0.928	368.7	-2.4
C3	1.080	0.992	0.835	0.909	1.188	0.918	371.7	-2.4
Average	1.069	0.994	0.836	0.898	1.190	0.930	373.4	-2.4
Range	4.2%	2.6%	0.7%	2.9%	2.0%	2.8%	3.0%	-1.9%

% change	0.4%	3.5%	2.6%	-0.7%	1.0%	3.2%	-5.7%	42.3%
----------	------	------	------	-------	------	------	-------	-------

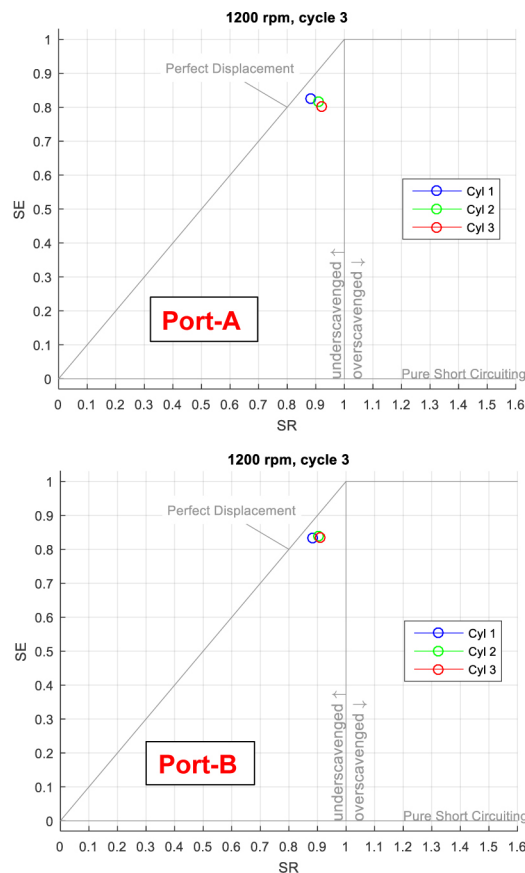


Figure 18. Scavenging efficiency for port-A and port-B from open-cycle CFD simulations.

Although port-B results in better scavenging, its impact on engine combustion and indicated thermal efficiency also needs to be compared to port-A. For the combustion system, a design of experiments (DOE) was carried out for both the ports. The combustion performance for the two ports was compared to determine the best combustion configuration for each port design over a range of compression ratios: ranging from 15.5 to 20.5. As discussed in the previous section, based on the first iteration of the 1-D to 3-D coupled simulation, which provided the scavenging performance of the ports, the second iteration was undertaken to improve the boundary conditions. The improved boundary conditions are shown in Table 8 for part-load, peak-torque and rated power conditions.

Table 8. Updated boundary conditions for part-load, rate-power and peak-torque conditions as obtained from 1-D model

Speed	Torque	Power	BMEP	Global AFR	EGR	Intake Pressure
RPM	N-m	kW	bar	-	%	bar
1200	1016	128	6.5	26.5	20	1.95
1200	2032	255	13	24.1	20	2.85
1800	1814	342	11.6	22	14.8	3.4

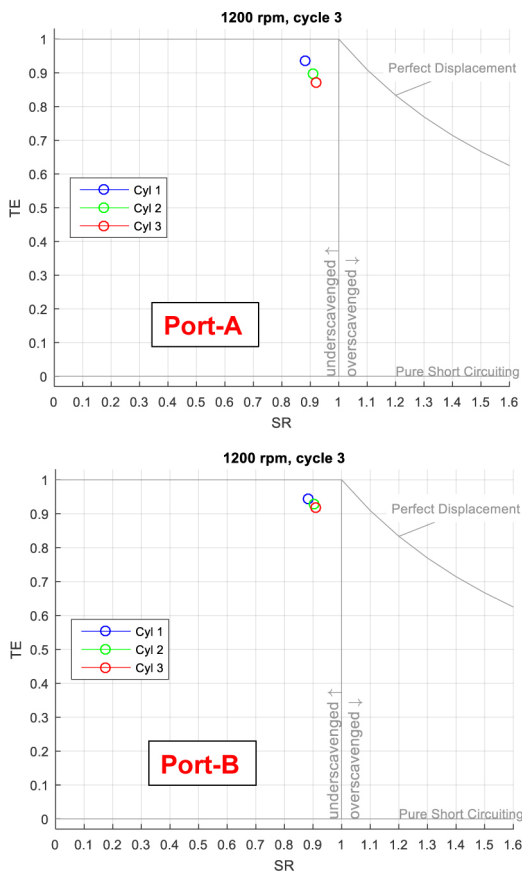


Figure 19. Trapping efficiency for port-A and port-B from open-cycle CFD simulations

Combustion System Optimization

The combustion system optimization includes a design of experiment (DOE) study that optimizes piston bowl shape parameters, injector design and trapped swirl ratio, which in turn dictate the port inclination angle for port-B. The optimization was carried out at part-load conditions to maximize indicated thermal efficiency that satisfies target emission levels. With the optimized combustion system, the resulting 9.8L engine was also simulated at rated-power and peak-torque conditions as well to predict engine performance. Commercial software MINITAB was used to construct a design of experiments model and make predictions. A range of piston bowl volume shapes were included in the study to account for range of compression ratio.

DOE Study

The latest generation of the Achates Power piston bowl shape was used in the DOE study, which resulted in high indicated thermal efficiency. A nine-factor DOE with central composite (CC) design with 160 runs was used to optimize the combustion system: factors shown in Table 9.

The nine factor DOE used in this work predicts the optimum condition by establishing a response surface from the input conditions, which in this work were generated by CFD simulation. It is likely that the optimum determined by the program is an interpolation between several of the input points which the program used to establish the response surface. Consequently, as an internal check and further refinement it is beneficial to run the full CFD for

the optimal operating condition predicted by the DOE. Figure 20 shows results from the DOE model predictor. The DOE model shows that port-B provides higher indicated thermal efficiency compared to port-A. This is primarily because of higher trapped swirl motion and lower trapped temperatures that results in higher trapped mass. Figure 21 shows validation of the DOE Model with the respective CFD predictions for indicated thermal efficiency. CFD validation of DOE predictions is necessary, especially when the DOE model selects values of factors towards the end limit of the range under investigation. CFD predictions show higher indicated thermal efficiency at higher compression ratio of 19 and 20 compared to DOE model predictions. Based on these results, port-B and high compression ratio bowl combination provides maximum ITE.

Table 9. DOE Factors for central composite design

DOE Factors for central composite design	
Compression Ratio	[-]
Swirl Ratio	[-]
Bowl parameter 1	[mm]
Bowl parameter 2	[mm]
Bowl parameter 3	[mm]
Spray Inclusion Angle	[deg.]
Hole size	[mm]
Rail Pressure	[bar]
Start of Injection	[deg. after minimum volume (aMinV)]

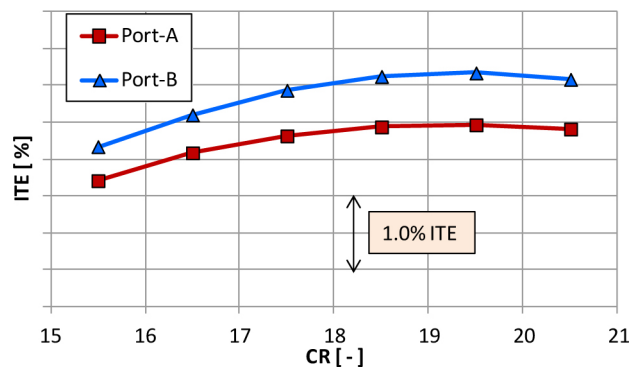


Figure 20. Combustion performance for two ports at various compression ratio obtained from DOE model predictions.

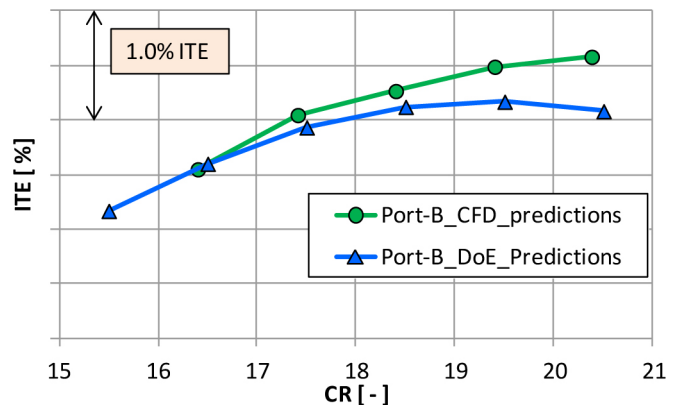


Figure 21. CFD prediction of combustion performance for port-B compared to DOE model prediction

The combustion system was optimized using a DOE model predictor for parameters with a constraint of constant engine-out NO_x . The optimized configuration for a 9.8L engine at part-load is shown in Table 10. The DOE model predictor shows that the best configuration

includes a combination of a larger nozzle hole size and a medium rail pressure based on the range considered in the study for these two factors. The optimum swirl for part-load condition is 2.4, which was achieved with a re-designed port-B geometry to that yield this swirl ratio at part-load conditions. CFD predictions of ITE at various compression ratios shows that the ITE continues to increase till a compression ratio of 20.5 as shown in [Figure 21](#).

Table 10. Optimized factors from DOE model predictor at a constant engine-out NOx.

Optimized Factors from DOE model	
Compression Ratio [-]	Towards Higher Limit
Swirl Ratio [-]	Mid Range
Bowl parameter 1 [mm]	Towards Lower Limit
Spray inclusion angle [deg.]	Towards Higher Limit
Bowl parameter 2 [mm]	Towards Higher Limit
Bowl parameter 3 [mm]	Towards Mid-Range
Hole size [mm]	Towards Higher Limit
Rail Pressure[bar]	Towards Mid-Range
Start of Injection [deg. aMinV]	Towards Delayed Limit

Results for Optimized Operating Conditions with Combustion System Optimized for Maximum ITE

To maximize BTE, a combination of hardware was considered: an optimized piston bowl shape, with trapped compression ratio toward higher limit, a thermal barrier coating on the piston bowls, and optimized injectors. SOI sweeps for this combustion system was simulated using combustion CFD at part-load, peak-torque and at rated-power conditions that provides ITE vs NOx trade-offs as shown in [Figure 22](#).

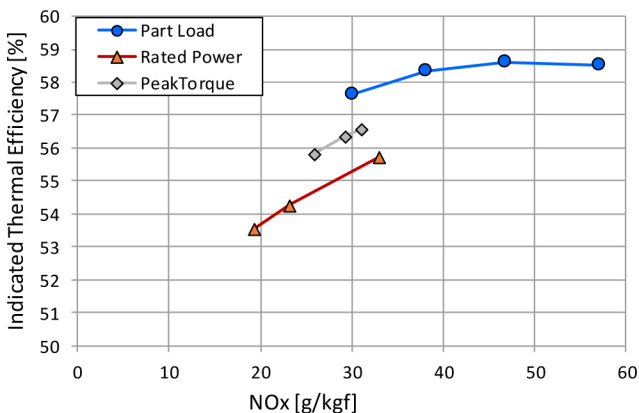


Figure 22. ITE vs NOx at Part-Load, Rated-Power and Peak-Torque for optimized combustion system obtained from combustion CFD simulations

[Figure 23](#) shows the variation of ITE for the start of injection timings for the two load-speed conditions. It can be observed that advancing start of injection timing to -10° after minimum volume (aMinV) does not improve ITE at part-load. At part-load, the maximum ITE of 58.6% is achieved at injection timing of -8° aMinV that gives engine-out NOx of 46.8 g/kgf. At peak-torque point, ITE of 55.8% is achieved at SOI of 0° aMinV. At rated power conditions, ITE of 53.6% is achieved at injection timing of -0.5° aMinV. [Figure 24](#) shows

in-cylinder pressure and heat released predictions for 9.8L engine for three load points, part-load at injection timing of -8° aMinV, rated-power at injection timing of -0.5° aMinV and peak-torque at injection timing of 0° aMinV, respectively. At rated-power and peak-torque conditions, start of injection is delayed relative to part-load conditions in order to keep PCP under 235 bar limit. [Table 11](#) shows combustion performance parameters as predicted from CFD simulations for the three load points.

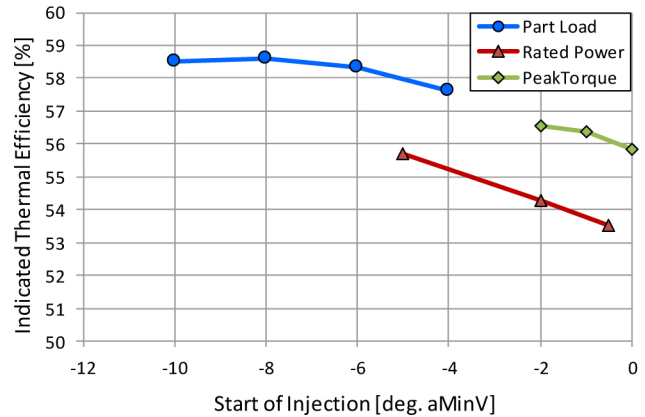


Figure 23. ITE vs Start of Injection timing injection for 9.8L engine Part-Load, Rated-Power and Peak-Torque for optimized combustion system obtained from combustion CFD simulations

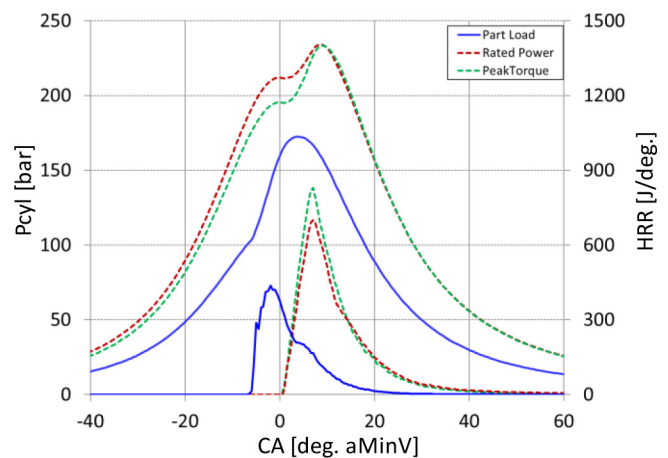


Figure 24. CFD predictions of in-cylinder pressure and instantaneous heat released rate at Part-Load, Rated-Power and Peak-Torque obtained from combustion CFD simulations

Table 11. CFD predictions of emission, burn duration and ITE at part-load, rated-power and peak-torque conditions for 9.8L engine obtained from combustion CFD simulations

9.8L_predictions				
Load	[-]	Part Load	Peak Torque	Rated Power
Engine Speed	[RPM]	1200	1200	1800
Soot	[g/kgf]	0.004	0.006	0.086
NOx	[g/kgf]	46.8	25.9	19.2
Pdv_CC	[kW]	51.1	97.0	131.6
CA10	[$^{\circ}$ aMinV]	-4.5	3.5	4.0
CA50	[$^{\circ}$ aMinV]	0.0	9.0	9.5
CA90	[$^{\circ}$ aMinV]	10.0	21.0	24.5
CA10-90	[$^{\circ}$ ca]	14.5	17.5	20.5
CC_ITE	[-]	56.9	54.2	52.0
ITE	[-]	58.6	55.8	53.5
PCP	[bar]	172.5	233.3	234.0

Friction Modeling and Predictions

A detailed friction model analysis was performed for the two-stroke OP 9.8L three-cylinder engine by using the analytical friction model that was validated for the 4.9L three-cylinder research engine, as discussed previously in this paper. The major components of the engine such as the pistons, bearings, crank train and gearbox were sized for a 235 PCP limit in order to establish the geometry required for the different sub-models of the friction model. The cylinder pressure trace obtained from GT-POWER was also used as an input for the friction model: [Figure 24](#). A lube and water system model was created in LMS AMESIM to determine flow rates and pressure requirements for the operating conditions as shown in [Table 5](#). Based on the assumption of a variable displacement pump, the flow and pressure requirement were converted in auxiliary power loss. The fuel pump power was calculated based on supplier data for the corresponding rail pressure, pump speed and fuel injection quantity. The predicted total friction power loss and breakdown can be seen in [Table 12](#). It can be seen that the predicted friction power loss for the production 9.8L in 2020 is expected to be much lower than the current measured friction of the 4.9L two-stroke OP research engine. A portion of this improvement is obtained from optimizing the engine design for friction - such as having an integrated gearbox with power take-off from exhaust crank, and optimized size and design of engine components. The remaining reduction in friction will be obtained by applying four-stroke technologies which have been published in literature and utilized in SuperTruck project. These include technologies listed below:

- Sputter coated bearings that are rated to unit loads of at least 120 MPa [\[36\]](#)
- Advanced piston ring coating that significantly reduce ring pack friction [\[37\]](#)
- Low friction polytetrafluoridethylene (PTFE) dynamic seals [\[38\]](#)

Table 12. Friction breakdown for 9.8L engine for part load and rated power point

Mode	Part Load	Peak Torque	Rated Power
Engine [rpm]	1200	1200	1800
Torque [N-m]	1016	2032	1814
Power [kW]	128	255	342
Friction Power loss in components [kW]			
Main bearings [kW]	0.9	1.2	2
Water pump [kW]	0.1	0.8	1.1
Lube Oil Pump [kW]	0.7	1.1	1.4
Fuel Pump [kW]	1.2	4.1	5.7
Seals [kW]	0.1	0.1	0.1
FEAD [kW]	0.6	0.8	1.1
Total Aux & Crank [kW]	3.6	8.1	11.4
Rod bearings [kW]	0.6	1	1.3
Piston Skirt [kW]	1.2	2.4	4.5
Piston rings [kW]	2.3	4.9	6.1
PC+rod [kW]	4.2	8.3	11.9
Windage [kW]	0.3	0.3	1.3
GB bearings [kW]	0.1	0.1	0.1
Gear mesh	0.6	1.3	1.6
GB+windage [kW]	0.9	1.7	3.1
Total Friction Power [kW]	8.7	18.1	26.4

BTE Predictions

The results from the combustion CFD (heat released rate and ITE) along with the friction power loss were input into the GT-POWER model. For the part-load condition, only the low pressure EGR is needed so the high pressure EGR valve was closed. Thus, the turbocharger efficiency was sufficient to deliver boost, airflow and EGR outlined in [Table 8](#) without requiring supercharger work. For the rated power point, only high pressure EGR was utilized, which results in approximately a 2.5% pumping losses. Engine out NO_x calculation is based on predicted NO_x from combustion CFD. With SCR conversion efficiency of 95.8% at part-load, 91.5% at rated power and 93.5% at peak-torque, the tailpipe emissions can be met. As discussed earlier, there is further possibility to improve performance at rated-power and peak-torque by lowering EGR as well as boost and advancing start of injection because of available margin in NO_x at these conditions. The combination of the thermal barrier coating, along with a liner designed to provide a trapped compression ratio of 21, and the unique combustion bowl of a two-stroke OP Engine can provide a maximum brake thermal efficiency of 55.0% for the 9.8L HD engine at part-load condition of 1200 rpm and 128 kW brake power. In addition, the engine delivers 342 kW of brake power with a brake thermal efficiency of 48.1% at rated-power and 255kW of brake power with a brake thermal efficiency of 50.8% at peak-torque conditions: with room for further optimization because of engine-out NO_x still within the target with margin of about 2-3 g/kW-hr. [Table 13](#) shows the prediction of pumping, friction loss and BTE for the two engine load points investigated. The 55% BTE corresponds to a 20% improvement compared to a heavy-duty 2014 DD15 multi-cylinder engine as published by National Highway Traffic Safety Administration (NHTSA) [\[39\]](#).

Table 13. Predictions of Pumping, Friction and BSFC for 9.8L engine at part-load, rated-power and peak torque conditions obtained from 1-D model coupled with 3-D combustion CFD and 3-D open-cycle CFD models

Engine Speed	RPM	1200	1200	1800
Engine BMEP	bar	6.5	13	11.6
Compressor Efficiency	%	79.0	80.5	78.9
Compressor Map PR	[-]	1.97	2.64	3.01
Turbine Efficiency (Aero + Mech)	%	73.2	68.8	64.1
Turbine Map PR	[-]	1.77	2.29	2.56
Turbine Rack Position	0-1	0.50	0.90	1.00
Total TC Efficiency	%	57.8	55.4	50.6
Supercharger Power	kW	0.0	5.2	9.2
BSFC	g/kW-hr	153.7	165.8	175.3
Engine Out BSNO _x	g/kW-hr	6.5	4.2	3.2
Desired SCR Conversion Efficiency	%	95.8	93.5	91.5
IMEP	bar	6.9	14.2	13.0
Average PCP	bar	172	229	235
Brake Power	kW	128	255	342
Brake Torque	Nm	1016	2032	1814
ITE	%	58.6	55.6	53.7
BTE	%	54.8	50.8	48.1
Friction/Fuel Power	%	3.7	3.7	4.3
Pumping/Fuel Power	%	0.0	1.0	1.3

Comparing OP Engine measured ITE of 52.5% for 4.9 L research engine with predicted 58.6% ITE for 9.8L heavy-duty engine, this increase can be attributed to primarily increase in trapped compression ratio from 15.4 to 21.0, increase in engine size and use of thermal barrier coating. The high efficiency results are achieved while maintaining an engine-out NO_x limit of 6.5 g/kW-hr at

1200rpm 6.5bar BMEP load, which is compatible with EPA 2010 emissions targets. These are the same targets for which the Department of Energy SuperTruck program was developed.

Given uncertainty in future emissions regulations, it should be noted that this technology alternatively can be optimized to much lower NO_x level to be compatible with future proposed tail-pipe emission of 0.027 g/kW-hr NO_x. The soot emissions from the same OP Engine will be within 0.015 g/kW-hr.

Summary/Conclusions

Opposed-Piston two-stroke engine models, viz., 3-D CFD, 1-D and friction models were correlated with measured data from dynamometer testing of a 4.9L three-cylinder research OP Engine. The correlated models match well the measurements and then were extended to predict the heavy-duty 9.8 L three-cylinder OP Engine performance. For the air handling system design, port optimization was performed; it was determined that smaller ports resulted in better scavenging performance. The combustion system was optimized using the design of experiment approach. CFD predictions at part-load at 1200 rpm show that an ITE of 58.4% can be achieved through use of a thermal barrier coating on both surfaces of the piston bowl. A 55% brake thermal efficiency is achieved at the part-load conditions. At rated conditions with engine speed of 1800 rpm, BTE of 48.1% is achieved and at peak-torque conditions at 1200 rpm, BTE of 50.8% is achieved.

The OP Engine offers a solution in reducing GHGs emission and reducing the carbon foot-print for 2020 and beyond. It is demonstrated that OP Engine will reduce fuel consumption by achieving best-point BTE of 55% without the use of costly addition of technologies such as waste heat recovery systems or additional turbo-compounding components.

References

1. "EPA and NHTSA Propose Greenhouse Gas and Fuel Efficiency Standards for Medium- and Heavy-Duty Trucks: By the Numbers", <https://www3.epa.gov/otaq/climate/documents/420f15903.pdf>, EPA-420-F-15-903, June 2015.
2. Delgado, O, and Lutsey, N., "The U.S. SuperTruck Program: Expediting the development of Advanced heavy-Duty Vehicle Efficiency Technologies", International Council of Clean Transportation, June 2014.
3. Koeberlein, D., "Technology and System Level Demonstration of Highly Efficient and Clean, Diesel Powered Class 8 Trucks," <http://energy.gov/eere/vehicles/vehicle-technologies-office-annual-merit-review-presentations>, Department of Energy report, project ID: ACE057, 2015.
4. Singh, S., "Recovery Act - Class 8 Truck Freight Efficiency Improvement Project", <http://energy.gov/eere/vehicles/vehicle-technologies-office-annual-merit-review-presentations>, Department of Energy report, project ID: ACE058, June 2015.
5. Zukouski, R., "SuperTruck - Development and Demonstration of a Fuel-Efficient Class 8 Tractor & Trailer Engine Systems", <http://energy.gov/eere/vehicles/vehicle-technologies-office-annual-merit-review-presentations>, Department of Energy report, project ID: ACE059, 2016.
6. Amar, P., Gibble, J., "SuperTruck Powertrain Technologies for Efficiency Improvement", <http://energy.gov/eere/vehicles/vehicle-technologies-office-annual-merit-review-presentations>, Department of Energy report, project ID: ACE060, 2016.
7. Hanson, R., Kokjohn, S., Splitter, D., and Reitz, R., "An Experimental Investigation of Fuel Reactivity Controlled PCCI Combustion in a Heavy-Duty Engine," *SAE Int. J. Engines* 3(1):700-716, 2010, doi:10.4271/2010-01-0864.
8. Kokjohn, S.L., Hanson, R.M., Splitter, D.A., and Reitz, R.D., "Fuel Reactivity Controlled Compression Ignition (RCCI): A Pathway to Controlled High-Efficiency Clean Combustion," *International Journal of Engine Research, Special Issue on Fuel Efficiency*, Vol. 12, pp. 209-226, 2011.
9. Hanson, R., Ickes, A., and Wallner, T., "Comparison of RCCI Operation with and without EGR over the Full Operating Map of a Heavy-Duty Diesel Engine," *SAE Technical Paper 2016-01-0794*, 2016, doi:10.4271/2016-01-0794.
10. Manente, V., Zander, C., Johansson, B., Tunestal, P. et al., "An Advanced Internal Combustion Engine Concept for Low Emissions and High Efficiency from Idle to Max Load Using Gasoline Partially Premixed Combustion," *SAE Technical Paper 2010-01-2198*, 2010, doi:10.4271/2010-01-2198.
11. Chang, J., Kalghatgi, G., Amer, A., Adomeit, P. et al., "Vehicle Demonstration of Naphtha Fuel Achieving Both High Efficiency and Drivability with EURO6 Engine-Out NO_x Emission," *SAE Int. J. Engines* 6(1):101-119, 2013, doi:10.4271/2013-01-0267.
12. Sharma, A. and Redon, F., "Multi-Cylinder Opposed-Piston Engine Results on Transient Test Cycle," *SAE Technical Paper 2016-01-1019*, 2016, doi:10.4271/2016-01-1019.
13. Regner, G., Herold, R., Wahl, M., Dion, E. et al., "The Achates Power Opposed-Piston Two-Stroke Engine: Performance and Emissions Results in a Medium-Duty Application," *SAE Int. J. Engines* 4(3):2726-2735, 2011, doi:10.4271/2011-01-2221.
14. Naik, S., Redon, F., Regner, G., and Koszewnik, J., "Opposed-Piston 2-Stroke Multi-Cylinder Engine Dynamometer Demonstration," *SAE Technical Paper 2015-26-0038*, 2015, doi:10.4271/2015-26-0038.
15. Redon, F., Kalebjian, C., Kessler, J., Rakovec, N. et al., "Meeting Stringent 2025 Emissions and Fuel Efficiency Regulations with an Opposed-Piston, Light-Duty Diesel Engine," *SAE Technical Paper 2014-01-1187*, 2014, doi:10.4271/2014-01-1187.
16. Venugopal, R., Abani, N., and MacKenzie, R., "Effects of Injection Pattern Design on Piston Thermal Management in an Opposed-Piston Two-Stroke Engine," *SAE Technical Paper 2013-01-2423*, 2013, doi:10.4271/2013-01-2423.
17. Herold, R., Wahl, M., Regner, G., Lemke, J. et al., "Thermodynamic Benefits of Opposed-Piston Two-Stroke Engines," *SAE Technical Paper 2011-01-2216*, 2011, doi:10.4271/2011-01-2216.

18. Dion, E. P., Lenski, B. M., and Mackenzie, R. G., "Piston constructions for opposed-piston engines" US 20120073526, 2012.
19. Senecal, P., Richards, K., Pomraning, E., Yang, T. et al., "A New Parallel Cut-Cell Cartesian CFD Code for Rapid Grid Generation Applied to In-Cylinder Diesel Engine Simulations," SAE Technical Paper [2007-01-0159](#), 2007, doi:[10.4271/2007-01-0159](#).
20. Patel, A., Kong, S., and Reitz, R., "Development and Validation of a Reduced Reaction Mechanism for HCCI Engine Simulations," SAE Technical Paper [2004-01-0558](#), 2004, doi:[10.4271/2004-01-0558](#).
21. Kong S.C., Sun Y., and Reitz R.D., Modeling diesel spray flame lift-off, sooting tendency and NOx emissions using detailed chemistry with phenomenological soot models, ASME J. Eng. Gas Turbines Power 129 (2007), pp. 245-251.
22. Smith G.P., Golden D.M., Frenklach M., Moriarty N.W., Eiteneer B., Goldenberg M., Bowman C.T., Hanson R.K., Song S., Gardiner W.C., Lissianski V.V., and Qin Z., 2000 [<http://www.me.berkeley.edu/gri-mech/>]
23. Hiroyasu, H. and Kadota, T., "Models for Combustion and Formation of Nitric Oxide and Soot in Direct Injection Diesel Engines," SAE Technical Paper [760129](#), 1976, doi:[10.4271/760129](#).
24. Nagle, J., and Strickland-Constable, R.F., "Oxidation of Carbon Between 1000-2000 C," Proceedings of the Fifth Carbon Conference, Vol. 1, p.154, 1962.
25. Patterson, M.A., "Modeling the Effects of Fuel Injection Characteristics on Diesel Combustion and Emissions," Ph.D. Thesis, University of Wisconsin-Madison, 1997.
26. Abani, N., and Reitz, R.D., "Diesel engine emissions and combustion predictions using advanced mixing models applicable to fuel sprays", Combustion Theory and Modelling, Vol. 14, Iss. 5, pp 715-746, 2010.
27. O'Rourke, P.J., "Collective Drop Effects on Vaporizing Liquid Sprays," Ph.D. Thesis, Princeton University, 1981.
28. Han, Z., and Reitz, R.D., "Turbulence Modeling of Internal Combustion Engines Using RNG k- ϵ Models," Combustion Science and Technology, Vol. 106, 1995.
29. Klyza, C., "Optical Measurement Methods used in Calibration and Validation of Modeled Injection Spray Characteristics," Poster P7, presented in the 2010 Directions in Engine-Efficiency and Emissions Research (DEER) Conference.
30. Abani, N., Kokjohn, S., Park, S., Bergin, M. et al., "An Improved Spray Model for Reducing Numerical Parameter Dependencies in Diesel Engine CFD Simulations," SAE Technical Paper [2008-01-0970](#), 2008, doi:[10.4271/2008-01-0970](#).
31. Taraza, D., Henein, N., Ceausu, R., and Bryzik, W., "Engine Friction Model for Transient Operation of Turbocharged, Common Rail Diesel Engines," SAE Technical Paper [2007-01-1460](#), 2007, doi:[10.4271/2007-01-1460](#).
32. Stanley, R., Taraza, D., Henein, N., and Bryzik, W., "A Simplified Friction Model of the Piston Ring Assembly," SAE Technical Paper [1999-01-0974](#), 1999, doi:[10.4271/1999-01-0974](#).
33. Taraza, D., Henein, N., and Bryzik, W., "Friction Losses in Multi-Cylinder Diesel Engines," SAE Technical Paper [2000-01-0921](#), 2000, doi:[10.4271/2000-01-0921](#).
34. Hersey, M. D., "Theory and Research in Lubrication: Foundations for Future Developments", pp. 44-47, John Wiley & Sons, 1966.
35. "Gears - Thermal capacity, Part 2: Thermal load-carrying capacity," ISO/TR 14179-2:2001(E), First edition 2001-08-01, ISO 2001, 2001.
36. Praca, M., Uehara, S., Ferreira, M., and Mian, O., "New Polymeric Coating on Sputtered Bearings for Heavy Duty Diesel Engines," *SAE Int. J. Engines* 6(1):623-628, 2013, doi:[10.4271/2013-01-1724](#).
37. Hoppe, S. and Kantola, T., "DuroGlide® - New Generation Piston Ring Coating for Fuel-Efficient Commercial Vehicle Engines," SAE Technical Paper [2014-01-2323](#), 2014, doi:[10.4271/2014-01-2323](#).
38. Reichert, J., and Schäfer, P., "Reduced Friction in Engine Sealing System for Truck Engines," MTZ World (2010) 71: 30. doi:[10.1007/BF03227989](#)
39. SwRI NHSTA 812194 report, <http://www.nhtsa.gov/Laws-&-Regulations/CAFE---Fuel-Economy/supporting-phase-2-proposal>, 2014.

Contact Information

Dr. Neerav Abani
Abani@achatespower.com

Address: 4060 Sorrento valley Blvd.,
 San Diego CA92121
 Tel: 858-535-9920

Acknowledgments

Authors would like to thank Dr. Dave Foster from University of Wisconsin-Madison, Dr. Gerhard Regner of Achates Power and John Koszewnik from Achates Power for continued discussions during the investigative study of Achates Power 9.8L heavy-duty OP Engine.

Abbreviations

OP - Opposed-Piston two-stroke

DOE - Design of Experiment

aMinV - after minimum volume

deg. aMinV - degrees after minimum volume

GHGs - Green House Gases

WHR - Waste Heat Recovery systems

ITE - Indicated Thermal Efficiency

BTE - Brake Thermal Efficiency

BMEP - Brake Mean Effective Pressure

FMEP - Friction Mean Effective Pressure

L/D ratio - Ratio of nozzle hole length and nozzle hole diameter

FEAD - Front End Accessory Drive

SE - Scavenging Efficiency

TE - Trapping Efficiency

DR - Delivery Ratio

SR - Scavenging Ratio

RC - Relative Charge

CE - Charging Efficiency

OEM - Original Equipment Manufacturer

PdV_CC - Closed-Cycle power generated calculated from port opening to port closure timings

CA10-90 - Burn Duration estimated as difference in crank angle degree timing at instant when 90% and 10% fuel chemical energy is released.

SOI - Start of Injection timing

PCP - Peak Cylinder Pressure

CAC - Charge Air Cooler

GB - Gear Box

DD15 - Detroit Diesel 15 ltr. engine

APPENDIX**APPENDIX-I**

Definition of various scavenging parameters are shown in following equations

$$\text{Delivery Ratio (DR)} = \frac{\text{Mass of delivered air}}{\text{Displaced volume} \times \text{Ambient density}}$$

$$\text{Trapping Efficiency (TE)} = \frac{\text{Mass of delivered air retained}}{\text{Mass of delivered air}}$$

$$\text{Scavenging Efficiency (SE)} = \frac{\text{Mass of delivered air retained}}{\text{Mass of trapped cylinder charge}}$$

$$\text{Relative Charge (RC)} = \frac{\text{Mass of trapped cylinder charge}}{\text{Displaced volume} \times \text{Ambient density}}$$

$$\text{Charging efficiency (CE)} = \frac{\text{Mass of delivered air retained}}{\text{Displaced volume} \times \text{Ambient density}}$$

$$\text{Scavenging Ratio (SR)} = \frac{\text{Mass of delivered air}}{\text{Mass of trapped cylinder charge}}$$

The Engineering Meetings Board has approved this paper for publication. It has successfully completed SAE's peer review process under the supervision of the session organizer. The process requires a minimum of three (3) reviews by industry experts.

All rights reserved. No part of this publication may be reproduced, stored in a retrieval system, or transmitted, in any form or by any means, electronic, mechanical, photocopying, recording, or otherwise, without the prior written permission of SAE International.

Positions and opinions advanced in this paper are those of the author(s) and not necessarily those of SAE International. The author is solely responsible for the content of the paper.

ISSN 0148-7191

<http://papers.sae.org/2017-01-0638>